10.10.2022

free ion (Spherical)

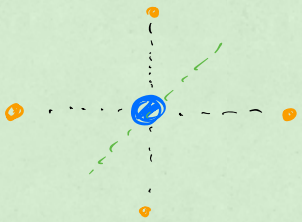

Non spherical symmetry

free ion ~eV

$$\mathcal{H} = \mathcal{H}_0 + \mathcal{H}_{ee}^{1} + \mathcal{H}_{SO} + \mathcal{H}_2$$

$\mathcal{H}_0 + \mathcal{H}_{ee}$: 1+2 Hund's rules

$\mathcal{H}_{SO}$: 10^{-2} eV

$\mathcal{H}_2$: 10^{-4} eV

$(3d)^4$ Mn^{3+}/Cr^{2+}

m	-2	-1	0	+1	+2
	↑	↑	↑	↑	—

$S = 4 \cdot \frac{1}{2} = 2$

$L = |\max(M)| = 2$

$J = |L-S| = 0$

$^5D_0$

$4f^{11}$ Er^{3+}

m	-3	-2	-1	0	+1	+2	+3
	↑↓	↑↓	↑↓	↑↓	↑	↑	↑

$S = \frac{3}{2}$

$L = |\max(M)| = 6$

$^{2S+1}[Name]_J = {}^4I_{15/2}$ ← Russel Saunders terms $|L, M, S, M_S\rangle$

Name	S	P	D	F	G	H	I	...
L	0	1	2	3	4	5	6	...

$J = L + S = \frac{15}{2}$

3rd Hund's rule (L, S) given

$$H_{so} = \sum_i \xi_{nl}\, \hat{s}_i \cdot \hat{l}_i \;\overset{\downarrow}{=}\; \lambda\, \hat{L}\cdot\hat{S}$$

$$\hat{J}^2 = (\hat{L}+\hat{S})^2 = \hat{L}^2 + \hat{S}^2 + 2\hat{S}\cdot\hat{L}$$

$$H_{so} = \frac{\lambda}{2}\left(\hat{J}^2 - \hat{L}^2 - \hat{S}^2\right)$$

$$\hat{J}^2 |J, M_J\rangle = J(J+1)\,|J, M_J\rangle$$

$$\hat{L}^2 |\ldots\rangle = L(L+1)\,|\ldots\rangle$$

$$\hat{S}^2 |\ldots\rangle = S(S+1)\,|\ldots\rangle$$

once L, S are defined by 1st & 2nd Hund's R.

$$\langle J M_J | H_{so} | J M_J\rangle = \frac{\lambda}{2}\left[J(J+1) - L(L+1) - S(S+1)\right]$$

favors

- small J values if $\lambda > 0$ — FILLING less than half
- large J values if $\lambda < 0$ — more than half

3rd Hund's rule

What can we say about $\vec{\mu}$ of free ions?

S, L, J determined $\Rightarrow |J, M_J\rangle$ basis

H_z as perturbation (1st order)

$$H_z = \sum_i B\mu_B (\hat{l}_i^z + g_e \hat{S}_i^z)$$

$$= B\mu_B (L^z + g_e S^z)$$

$$\langle J M_J | \hat{L}^z | J M_J \rangle = ?$$

i.e., it is proportional to B. These results are known as the *anomalous* Zeeman effect, counterposed to the normal Zeeman effect. The second one is observed when only the orbital angular momentum contributes to the Zeeman energy and no contribution comes from spin coordinates. This definition dates back to the end of the nineteenth century, when the spin had not been discovered yet: With today's knowledge, there is nothing anomalous in the anomalous Zeeman effect.

Equation (1.81) reproduces the magnetic moments of rare-earth ions fairly well, but not those of transition-metal ions in the solids. In the next chapter, we will see that this is due to the partial or total quenching of the angular momentum, which typically occurs when a transition-metal ion is hosted in a solid.

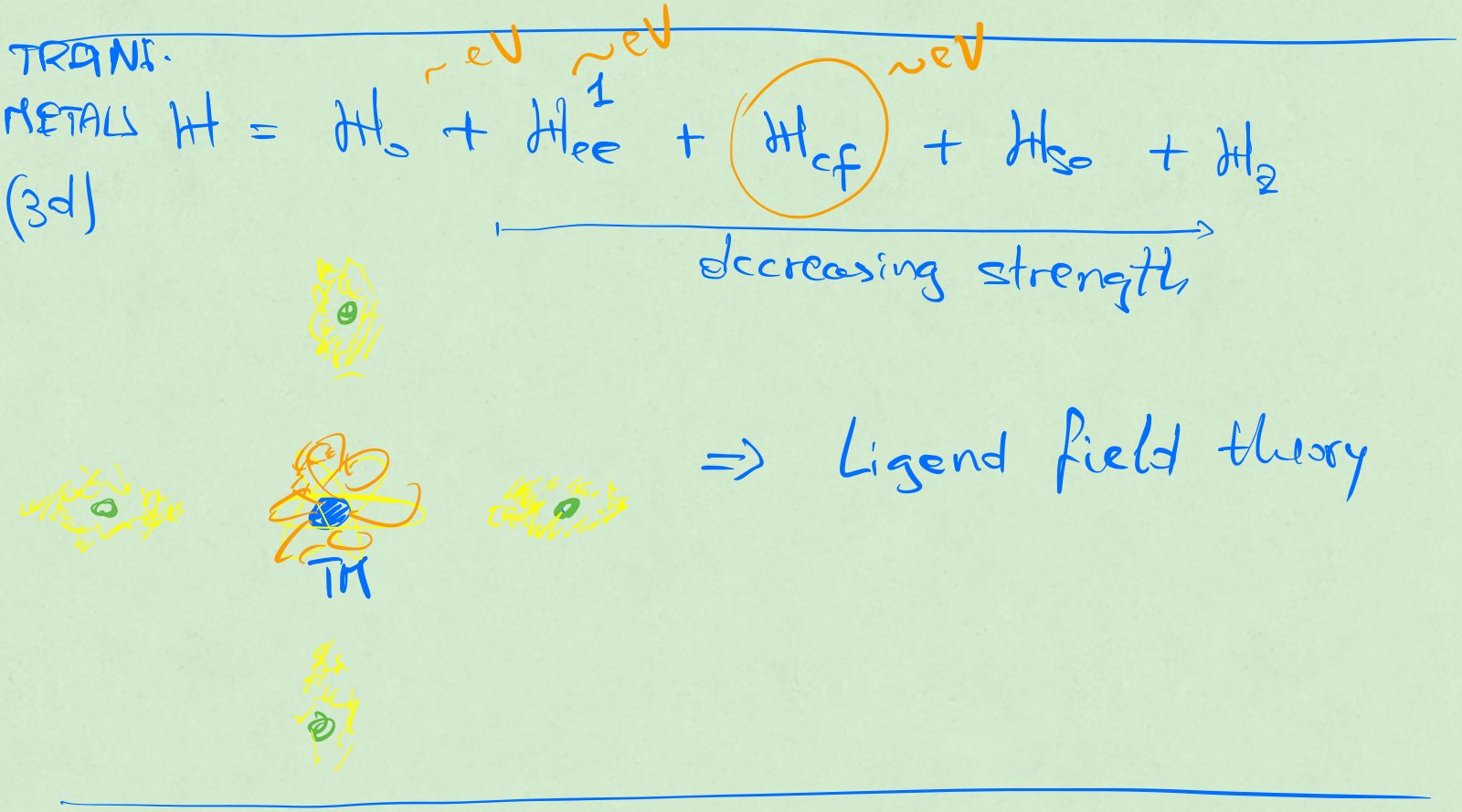

Chapter 2

Transition-metal and rare-earth ions in solids

Lecture: 10.10.2022

2.1 Transition-metal ions in crystals

When an atom is embedded in a solid, the main difference with respect to the free ion is that electrons are also affected by the electrostatic potential created by charges outside the atom itself. The aim of *ligand-field theory* is that of evaluating the effect of neighboring atoms – referred to as *ligands* – on the energy levels of the atom under consideration. Within this theory, the effect of the ligands is taken into account by the symmetry and the strength of the electric field produced by them. In its original formulation, developed by Bethe in 1929, ligands were treated as point charges[1]. With this simplification, the approach goes under the name of *crystal-field theory*. Already from the first attempts to turn the Bethe approach into a quantitative calculation, it was clear that it produced a splitting of the energy levels of transition-metal ions far smaller than the one observed in experiments. Van Vleck (1935) demonstrated that this mismatch originated from neglecting the overlap between the paramagnetic-ion orbitals and the ligand valence orbitals[1].

In transition metals the magnetic orbitals (i.e., the 3d orbitals containing unpaired electrons) are rather delocalized and have a comparatively high degree of covalency, namely they participate in the chemical bonding. For these reasons the magnetic d orbitals are strongly affected by the crystal-field interaction and the strength of this interaction is comparable to the intra-atomic

$n, \ell,$

$3d \quad (n, \ell) = (3, 2)$

$4f \quad (n, \ell) = 4, 3$

exchange interaction (1-2 eV). In other words, the crystal-field interaction is stronger than the spin-orbit coupling. The hierarchy of contributions to the Hamiltonian of a transition-metal ion reads

$$\mathcal{H} = \mathcal{H}_0 + \mathcal{H}^1_{\rm ee} + \mathcal{H}_{\rm cf} + \mathcal{H}_{\rm so} + \mathcal{H}_{\rm Z}\,. \tag{2.1}$$

As seen in Section (1.3), the Hamiltonian $\mathcal{H}_0$ on the r.h.s. of Eq. (2.1) includes the kinetic energy of electrons of the atom, their Coulomb interaction with the nucleus, and the part of electron-electron repulsion that can be written as a central potential. The orbital eigenstates of the $\mathcal{H}_0$ are the same as those of the hydrogen atom. If terms of higher order than $\mathcal{H}_0$ are neglected in the electronic Hamiltonian $\mathcal{H}$, the spin and orbital eigenstates can be expressed on a basis of mutually commuting operators: the hydrogen-like Hamiltonian ($\mathcal{H}_0$), $\hat{\mathbf{L}}^2$, $\hat{\mathbf{S}}^2$, $\hat{L}^z$, $\hat{S}^z$. These eigenstates are called Russell-Saunders terms. A perturbative treatment of the remaining contribution of the electron-electron repulsion ($\mathcal{H}^1_{\rm ee}$) removes part of the degeneracy and defines a ground-state multiplet consistent with the first two Hund's rules. The next contributions on the right-hand side of Eq. (2.1) represent the crystal-field interaction ($\mathcal{H}_{\rm cf}$), the spin-orbit coupling ($\mathcal{H}_{\rm so}$) and the Zeeman energy ($\mathcal{H}_{\rm Z}$). In transition-metal ions the strength of interactions on the r.h.s. of Eq. (2.1) decreases from left to right. We will see that in rare-earth ions the relative position of $\mathcal{H}_{\rm cf}$ and $\mathcal{H}_{\rm so}$ is swapped.

Crystal-field theory for 3d ions

In the following pages we sketch an instructive calculation[1] that estimates how the free-ion energy levels are split due to the presence of the ligands. As we do not aim at quantitative predictions, we will treat ligands as point charges (*crystal-field theory*). We will restrict ourselves to placing these point charges – which mimic the effect of the orbitals of neighboring atoms – at the corners of a square (Fig. 2.1) or at the vertices of an octahedron (Fig. 2.2) in which a magnetic d ion is supposed to be embedded. These tutorial examples are, nevertheless, of relevance in nowadays research. To the first order in perturbation theory, the effect of crystal-field interaction on single-electron levels can be expressed through the matrix elements

$$\langle l', m'|\mathcal{H}_{\rm cf}|l, m\rangle\,, \tag{2.2}$$

[1] More details about this calculation can be found in the book *Inorganic Electronic Structure and Spectroscopy*, Vol. I: Methodology, Editors: E. I. Solomon and A. B. P. Lever (1999, John Wiley and Sons, Inc.) Chapter: "Ligand Field Theory and the Properties of Transition Metal Complexes".

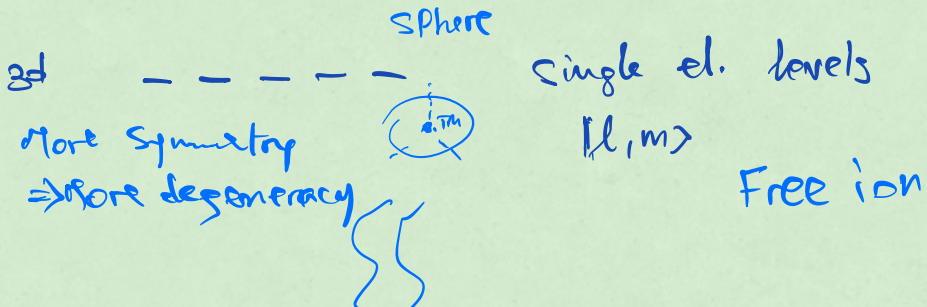

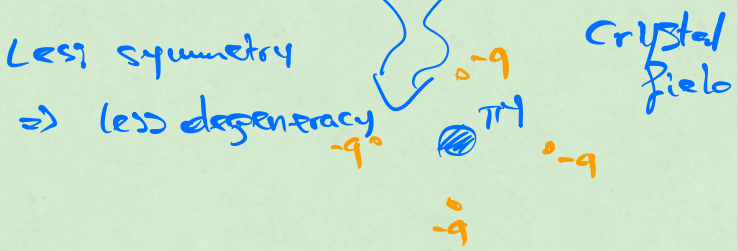

where l and m are the quantum numbers associated with $\hat{\mathbf{l}}^2$ and $\hat{l}^z$ for one electron in a d orbital, namely they represent single-electron levels. Since the principal quantum number n is the same for all the d levels, it has been omitted for simplicity of notation. The spin has also been neglected because $\mathcal{H}_{\rm cf}$ does not affect spin coordinates directly. The advantage of using point charges is that the potential associated with the electric field generated by one ligand onto the considered 3d ion can be expanded in spherical harmonics. Taking the nucleus of the paramagnetic ion as the origin of coordinates, the Coulomb energy associated with the interaction of the electron i with the point-like ligand h of charge $Z_h e$ is

$$\mathcal{H}_{{\rm cf},h} = \frac{Z_h e^2}{4\pi\epsilon_0}\frac{1}{|\underline{r}_i - \underline{r}_h|} = \frac{Z_h e^2}{4\pi\epsilon_0}\sum_{k=0}^{\infty}\frac{4\pi}{2k+1}\sum_{q=-k}^{k}\left[Y^*_{k,q}(\theta_h,\phi_h)\,\frac{r_i^k}{r_h^{k+1}}\,Y_{k,q}(\theta_i,\phi_i)\right] . \tag{2.3}$$

The spherical harmonics that are functions of the angular coordinates of the ligand are highlighted in blue. Summing this potential over all the ligands labeled by h gives the total energy of the crystal-field Hamiltonian acting on the i-th electron: $\mathcal{H}_{\rm cf} = \sum_h \mathcal{H}_{{\rm cf},h}$. The dependence of $\mathcal{H}_{{\rm cf},h}$ on the angular coordinates of the i-th electron put restrictions on the possible values of k. Eventually, we will have to evaluate matrix elements of the type given in Eq. (2.2), containing terms like

$$\langle l', m'|Y_{k,q}(\theta_i,\phi_i)|l,m\rangle \sim \int Y^*_{l',m'}(\theta_i,\phi_i)\,Y_{k,q}(\theta_i,\phi_i)\,Y_{l,m}(\theta_i,\phi_i)\,d\Omega_i\,. \tag{2.4}$$

where the integral is performed over the solid angle $d\Omega_i = \sin\theta_i\, d\theta_i\, d\phi_i$. For d orbitals ($l = 2$) such terms vanish for $k > 4$, therefore we can restrict ourselves to $k \le 4$[2].

Let us start focusing on a square planar complex, associated with the D_{4h} point group (see Fig. 2.1). The symmetry elements of the group impose additional restrictions to the spherical harmonics that are allowed in the expansion of $\mathcal{H}_{{\rm cf},h}$, so that the most general crystal-field Hamiltonian for a square planar arrangement of ligands reads

$$\begin{aligned}\mathcal{H}_{D_{4h}} = {} & \gamma_2^0\,\rho^2\,Y_{2,0}(\theta_i,\phi_i) + \gamma_2^2\,\rho^2\,\left[Y_{2,2}(\theta_i,\phi_i) + Y_{2,-2}(\theta_i,\phi_i)\right] \\ & + \gamma_4^0\,\rho^4\,Y_{4,0}(\theta_i,\phi_i) + \gamma_4^2\,\rho^4\,\left[Y_{4,2}(\theta_i,\phi_i) + Y_{4,-2}(\theta_i,\phi_i)\right] \\ & + \gamma_4^4\,\rho^4\,\left[Y_{4,4}(\theta_i,\phi_i) + Y_{4,-4}(\theta_i,\phi_i)\right] .\end{aligned} \tag{2.5}$$

[2]For the same reason, in the case of rare-earths metals, in which the magnetic contribution is provided by partially filled f orbitals ($l = 3$), one would have to consider $k \le 6$.

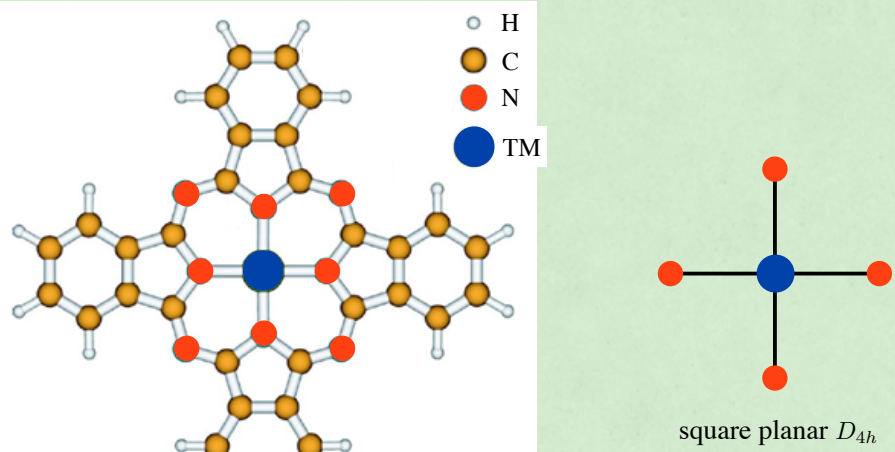

Figure 2.1: Left: Structure of the TM-Phthalocyanine molecule (with formula $(C_8H_4N_2)_4TM$) where TM=transition metal. Right: Illustration of the crystal-field approximation in which the effect of the four nitrogen atoms surrounding the TM ions is modeled with negative point charges (red balls).

where $\rho = r_i/a$ with a distance between each ligand and the nucleus of the transition-metal (TM) ion, thought in the center of a square (Fig. 2.1 right); the γ_k^q coefficients (highlighted in blue for convenience) depend on the ligand angular coordinates

$$\gamma_k^q = \frac{4\pi}{2k+1}\frac{Z_h e^2}{4\pi\epsilon_0}\frac{1}{a}\sum_h Y_{k,q}(\theta_h,\phi_h) \tag{2.6}$$

and have the units of an energy. For this specific geometry it is $\theta_h = \pi/2$ for every ligand and $\phi_h = 0, \pi/2, \pi, 3\pi/2$. The value of each γ_k^q coefficient is obtained inserting the appropriate spherical harmonic and summing over all the ligands. Assuming the charge $Z_h e^2$ to be the same for each ligand, for instance, the coefficient γ_2^0 is obtained as follows

$$\begin{aligned}\gamma_2^0 &= \frac{4\pi}{5}\frac{Z_h e^2}{4\pi\epsilon_0}\frac{1}{a}\frac{1}{4}\sqrt{\frac{5}{\pi}}\sum_h\left(3\cos^2\theta_h - 1\right)\\ &= -4\sqrt{\frac{\pi}{5}}\frac{Z_h e^2}{4\pi\epsilon_0}\frac{1}{a}\,.\end{aligned} \tag{2.7}$$

Any other coefficient can be determined performing the sum $\sum_h$ of the trigonometric function corresponding to the specific spherical harmonic evaluated on the four ligands. Apart from constant prefactors, this trigonometric contribution to the γ_k^q coefficients that are relevant for the planar D_{4h} geometry are computed in Table 2.1

Matrix elements of $\mathcal{H}_{D_{4h}}$: operator-equivalence method

In this paragraph we will evaluate explicitly the matrix elements of the crystal-field Hamiltonian on the single-electron basis $|l, m\rangle$. This task is facilitated by expressing the spherical harmonics that are functions of the electron coordinates in terms of Racah tensor operators

$$C_k^q = \sqrt{\frac{4\pi}{2k+1}} Y_{k,q} \tag{2.8}$$

where k is the rank of the tensor and q its component. Note that we have omitted the explicit dependence on the coordinate (θ_i, ϕ_i) because this more abstract representation will turn out to be useful. The reader who feels uncomfortable with this notation can always think of the C_k^q operators in real space, where they are just functions of (θ_i, ϕ_i) proportional to the spherical harmonics, as defined in Eq. (2.8). In terms of the C_k^q operators, the crystal-field Hamiltonian $\mathcal{H}_{D_{4h}}$ can be expressed in a very compact way

$$\mathcal{H}_{D_{4h}} = 21Dq \left[C_4^0 + \sqrt{\frac{5}{14}} \left(C_4^4 + C_4^{-4} \right) \right] - 21Dt\, C_4^0 - 7Ds\, C_2^0 , \tag{2.9}$$

in which the crystal-field coefficients Dq, Dt, and Ds contain the numerical factors arising from the sum over the γ_k^q indices associated with each ligand (see Table 2.1) and the average of r_i with respect to the radial part of the single-electron wave function $R_{nl}(r_i)$. We give the crystal-field coefficients for the more general case of a 3d complex associated with a D_{4h} symmetry, in which the point-charge ligands occupy the vertices of a compressed/elongated octahedron:

$$Dq = \frac{1}{6} \frac{Z_h e^2}{4\pi\epsilon_0} \frac{\bar{r^4}}{a^5} \qquad Ds = \frac{2}{7} \frac{Z_h e^2}{4\pi\epsilon_0} \left(\frac{\bar{r^2}}{a^3} - \frac{\bar{r^2}}{b^3} \right) \qquad Dt = \frac{2}{21} \frac{Z_h e^2}{4\pi\epsilon_0} \left(\frac{\bar{r^4}}{a^5} - \frac{\bar{r^4}}{b^5} \right) \tag{2.10}$$

The length b represents the distance between the nucleus of the TM ion and the ligands positioned on the axis perpendicular to the xy plane (Fig. 2.2 right). The bar indicates the average over the radial coordinates. If the "b" terms are omitted, the crystal field generated by a planar square geometry

is obtained (Fig. 2.1). For $b = a$, instead, one has $Dt = Ds = 0$; this limit corresponds to the perfect octahedral symmetry (O_h point group, illustrated in Fig. 2.2 left).

To determine how the degenerate levels $|l, m\rangle$ – originating from the $\mathcal{H}_0$ Hamiltonian – are split by the effect of the crystal field, one has to calculate the matrix elements of the Racah C_k^q operators on the basis $|l, m\rangle$. Using the Wigner-Eckart theorem and other elegant results of tensor algebra, the following equation is obtained

$$\langle l', m'|C_k^q|l, m\rangle = (-1)^{m'}\sqrt{(2l+1)(2l'+1)}\begin{pmatrix} l' & k & l \\ 0 & 0 & 0 \end{pmatrix}\begin{pmatrix} l' & k & l \\ m' & q & -m \end{pmatrix} \tag{2.11}$$

where the term in parenthesis are just numerical coefficients called 3-j Wigner symbols. Nowadays routines to compute the 3-j symbols are available in standard environments, like Mathematica and Matlab, or even from online calculators. A 3-j symbol is zero if the sum of the components in the bottom raw $(m' + q - m)$ is not zero, which restricts the coefficients that are to be computed explicitly. In the end, only the following non-zero terms remain

$$\begin{aligned}
&\langle 2, 2|C_4^0|2, 2\rangle = \langle 2, -2|C_4^0|2, -2\rangle = \frac{1}{21} \\
&\langle 2, 1|C_4^0|2, 1\rangle = \langle 2, -1|C_4^0|2, -1\rangle = -\frac{4}{21} \\
&\langle 2, 0|C_4^0|2, 0\rangle = \frac{2}{7}
\end{aligned}$$

$$\begin{aligned}
&\langle 2, 2|C_2^0|2, 2\rangle = \langle 2, -2|C_2^0|2, -2\rangle = -\frac{2}{7} \\
&\langle 2, 1|C_2^0|2, 1\rangle = \langle 2, -1|C_2^0|2, -1\rangle = \frac{1}{7} \\
&\langle 2, 0|C_2^0|2, 0\rangle = \frac{2}{7}
\end{aligned} \tag{2.12}$$

$$\langle 2, -2|C_4^4|2, 2\rangle = \langle 2, 2|C_4^{-4}|2, -2\rangle = \sqrt{\frac{10}{63}}\,.$$

The last ones are the only off-diagonal matrix elements (highlighted in blue). We have now all what we need to compute the desired matrix elements which are given in Table 2.2. The eigenvalues of that matrix give the correction to the energies of the five levels $|l, m\rangle$ that are degenerate with respect to the Hamiltonian $\mathcal{H}_0$. The crystal-field Hamiltonian $\mathcal{H}_{D_{4h}}$ generally removes this degeneracy leaving only one pair of levels with the same energy. However, in

			γ_2^0	$\gamma_2^{\pm 2}$	γ_4^0	$\gamma_4^{\pm 2}$	$\gamma_4^{\pm 4}$
Ligand	θ_h	ϕ_h	$3\cos^2\theta_h - 1$	$\sin^2\theta_h e^{\pm 2i\phi_h}$	$35\cos^4\theta_h - 30\cos^2\theta_h + 3$	$\sin^2\theta_h(7\cos^2\theta_h - 1)e^{\pm 2i\phi_h}$	$\sin^4\theta_h e^{\pm 4i\phi_h}$
1	$\pi/2$	0	-1	1	3	1	1
2	$\pi/2$	$\pi/2$	-1	-1	3	-1	1
3	$\pi/2$	π	-1	1	3	1	1
4	$\pi/2$	$3\pi/2$	-1	-1	3	-1	1
Sum			-4	0	12	0	4

Table 2.1: Contribution to the γ_k^q coefficients arising from the trigonometric functions contained in the spherical harmonics (second raw) evaluated on the different ligands of the planar D_{4h} geometry. The sum over all the ligands is given in the last raw. Normalization constants of the $Y_{k,q}(\theta_h, \phi_h)$ functions and numerical prefactors present in Eq. (2.6) are not considered for clarity.

$\mathcal{H}_{D_{4h}}$	$\|2,2\rangle$	$\|2,1\rangle$	$\|2,0\rangle$	$\|2,-1\rangle$	$\|2,-2\rangle$
$\langle 2,2\|$	$Dq - Dt + 2Ds$	0	0	0	$5Dq$
$\langle 2,1\|$	0	$-4Dq + 4Dt - Ds$	0	0	0
$\langle 2,0\|$	0	0	$6Dq - 6Dt - 2Ds$	0	0
$\langle 2,1\|$	0	0	0	$-4Dq + 4Dt - Ds$	0
$\langle 2,-2\|$	$5Dq$	0	0	0	$Dq - Dt + 2Ds$

Table 2.2: Matrix elements of the crystal-field Hamiltonian $\langle l', m'|\mathcal{H}_{D_{4h}}|l, m\rangle$ for an arrangement of ligands consistent with the D_{4h} point group in 3D, namely with point charges disposed on an elongated/compressed octahedron.

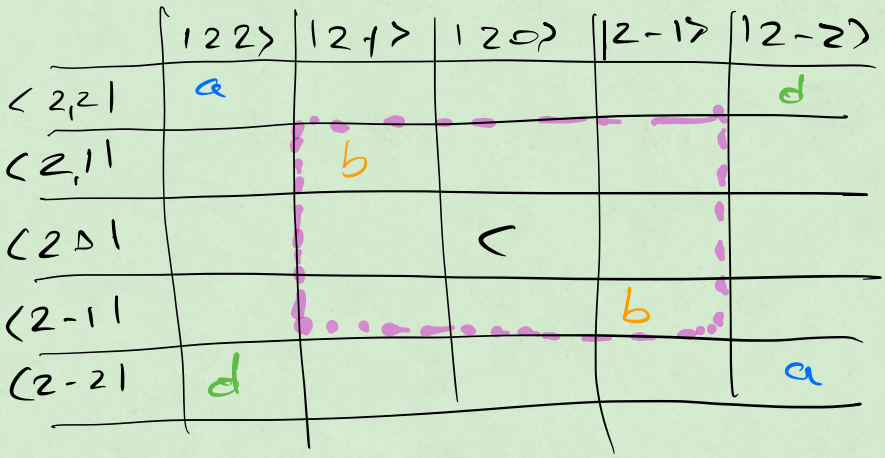

Subspace $|2,2\rangle, |2,-2\rangle$

	$\|2\ 2\rangle$	$\|2\ -2\rangle$
$\langle 2\ 2\|$	a	d
$\langle 2\ -2\|$	d	a

$$\begin{pmatrix} a & d \\ d & a \end{pmatrix} \begin{pmatrix} 1 \\ \pm 1 \end{pmatrix} = (a \pm d) \begin{pmatrix} 1 \\ \pm 1 \end{pmatrix}$$

eig

$a+b$ $\quad d_{x^2-y^2} = \frac{1}{\sqrt{2}}\left[|2,2\rangle + |2,-2\rangle\right]$

$a-b$ $\quad d_{xy} = \frac{i}{\sqrt{2}}\left[|2\ 2\rangle - |2,-2\rangle\right]$

Subspace $|2,1\rangle$ $|2\ 0\rangle$ $|2,-1\rangle$

$d_{z^2} = |2,0\rangle$

$d_{xz} =$

$d_{yz} =$

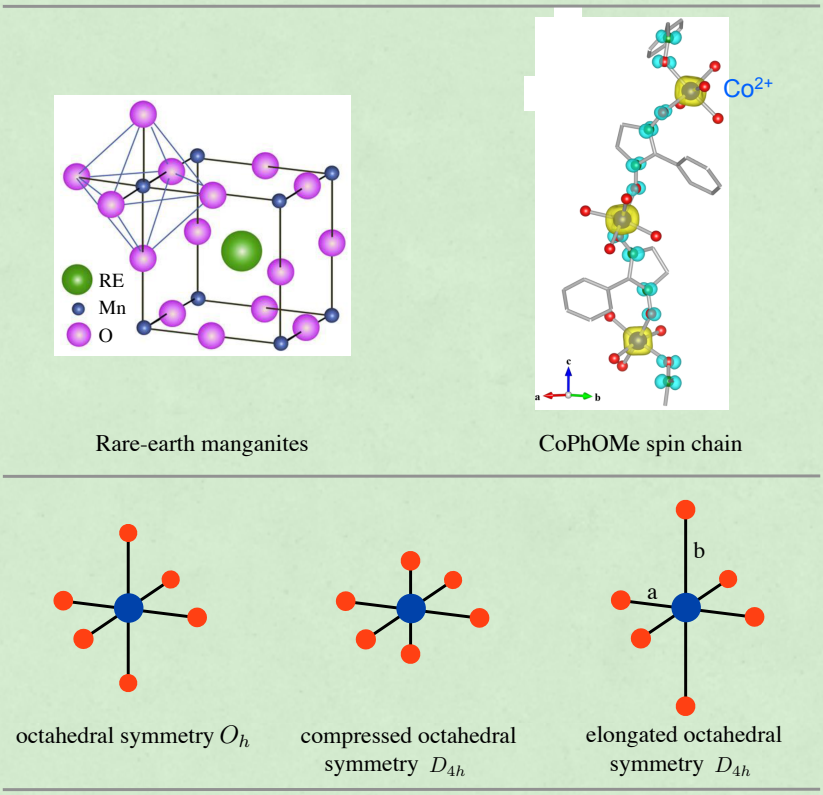

Figure 2.2: Top: Structure of a generic rare-earth manganite (left), $REMnO_3$, where RE=rare-earth metal, and of the $Co(hfac)_2$(NITPhOMe) spin chain – shortened as CoPhOMe in the figure; the yellow shadowed region indicates the spin density obtained from DFT calculations. In both cases the magnetic properties of the transition-metal ions are crucially affected by the environment of ligands in distorted octahedral symmetry (D_{4h} group). Bottom: Illustration of the octahedral crystal-field associated with the O_h and the D_{4h} point groups. Negative point charges (red balls) lie at the vertices of a Platonic octahedron (left) or of compressed (center) and elongated octahedra (right). The corresponding symmetry groups O_h and D_{4h} are also indicated.

the most symmetric case of octahedral symmetry (O_h group), the five levels $|l, m\rangle$ are split only into two multiplets, with degeneracy 2 and 3.

Orbital degeneracy and quenching of $\hat{\mathbf{L}}$

The matrix $\langle l', m'|\mathcal{H}_{\rm cf}|l, m\rangle$ given in Table 2.2 can easily be diagonalized. The resulting eigenvectors are directly related to the irreducible representations of the D_{4h} group. In other words, they are determined by the symmetry of the ligands surrounding the transition-metal ion under consideration. For this reason, these eigenvectors are called *symmetry-adapted wave functions* and, for the specific case of the matrix $\langle l', m'|\mathcal{H}_{\rm cf}|l, m\rangle$ obtained from the Racah oprators Eq. (2.12), are the so-called real d orbitals

$$\begin{aligned} d_{x^2-y^2} &= \frac{1}{\sqrt{2}}\left[|2,+2\rangle + |2,-2\rangle\right] \\ d_{z^2} &= |2,0\rangle \\ d_{xy} &= -\frac{i}{\sqrt{2}}\left[|2,+2\rangle - |2,-2\rangle\right] \\ d_{xz} &= -\frac{1}{\sqrt{2}}\left[|2,+1\rangle - |2,-1\rangle\right] \\ d_{yz} &= \frac{i}{\sqrt{2}}\left[|2,+1\rangle + |2,-1\rangle\right] . \end{aligned} \tag{2.13}$$

The real d orbitals are linear combinations of single-electron orbitals $|l, m\rangle$ with $l = 2$ and $m = -2, -1, 0, +1, +2$ (spherical harmonics in the real space). A 3D representation of the real d orbitals is given in the Assignments but can easily be found it also on the web. The perfect octahedral symmetry (O_h) corresponds to choosing $Dt = Ds = 0$ in the matrix given in Table 2.2. In this special case, that matrix has only two distinct eigenvalues:

$$\begin{aligned} E_{e_g} &= 6Dq \\ E_{t_{2g}} &= -4Dq\,, \end{aligned} \tag{2.14}$$

two-fold (e_g) and three-fold (t_{2g}) degenerate, respectively. The t_{2g} triplet is composed by the orbitals d_{xy}, d_{xz} and d_{yz}, which lie at lower energy in perfect octahedral environment (O_h symmetry group). The orbitals d_{z^2} and $d_{x^2-y^2}$, instead, form the e_g doublet placed at higher energy (see Fig. 2.3 middle).

We now evaluate the matrix elements of the orbital part of the Zeeman Hamiltonian for the i-th electron

$$\mathcal{H}^l_{{\rm Z},i} = \mu_{\rm B}\,\hat{\mathbf{l}}_i \cdot \vec{B} = \mu_{\rm B}\,B\,\hat{l}^z_i\,, \tag{2.15}$$

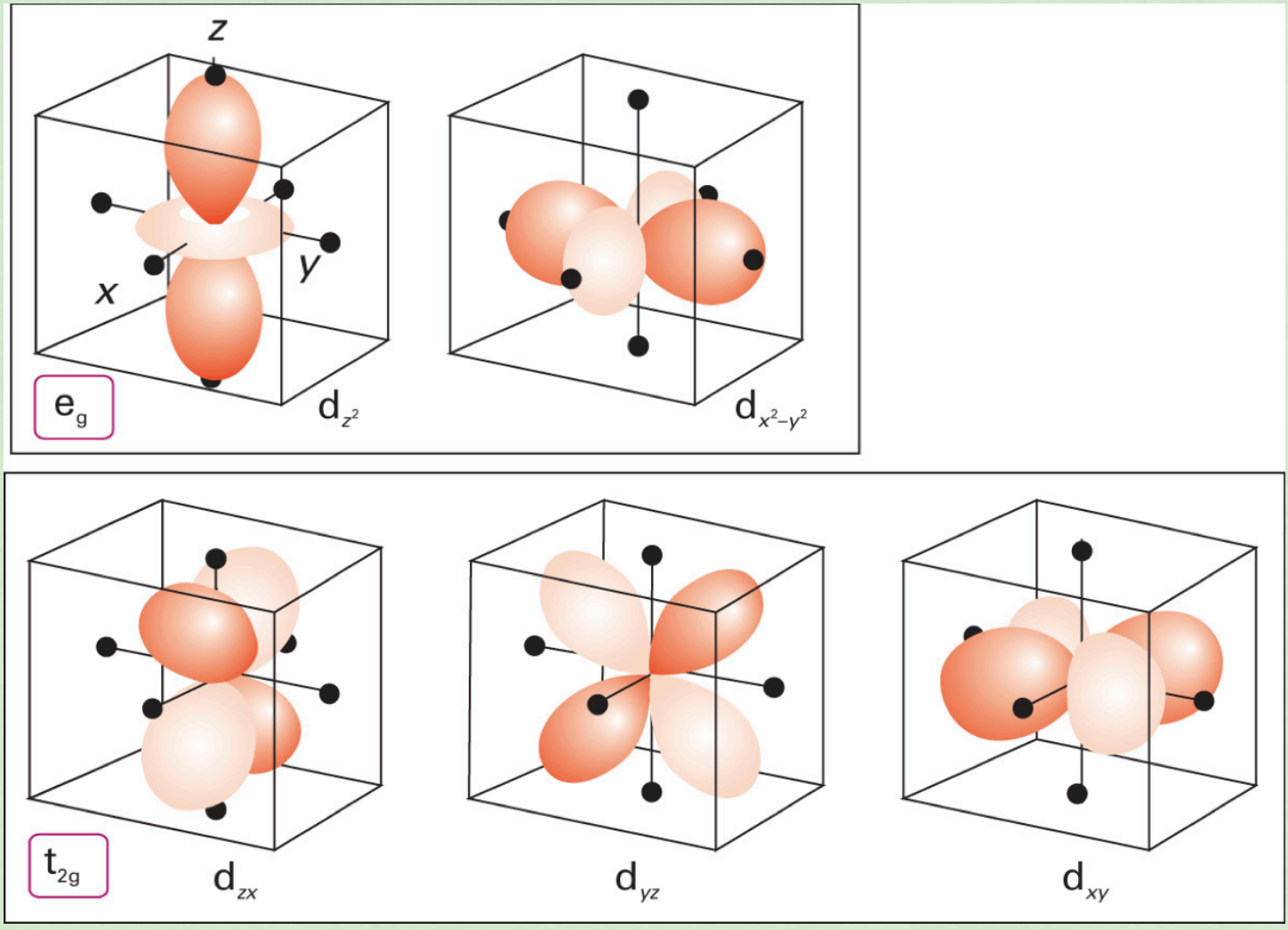
z
x
y
e_g
d_{z^2}
$d_{x^2-y^2}$
t_{2g}
d_{zx}
d_{yz}
d_{xy}

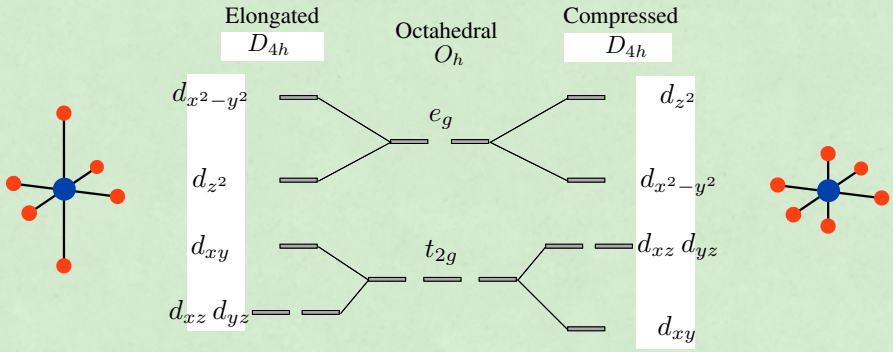

Figure 2.3: Splitting of the energies levels e_g and t_{2g} – characterizing a crystal-field Hamiltonian associated with a perfect octahedral symmetry – produced by compression/elongation of the ligand octahedron. Both operations reduce the symmetry from O_h to D_{4h}.

assuming the external field $\vec{B}$ to be applied along the z axis. When $B = 0$, the configuration with lower energy can be obtained placing the electron i in *any* of the d_{xy}, d_{xz} and d_{yz} orbitals defining the t_{2g} multiplet, the energy of these three configurations being $E_{t_{2g}}$. When $B \neq 0$, the matrix elements of the Hamiltonian $\mathcal{H}_0 + \mathcal{H}_{\rm cf} + \mathcal{H}_{\rm Z}$ evaluated within the t_{2g} multiplet read

$\mathcal{H}_0 + \mathcal{H}_{\rm cf} + \mathcal{H}_{\rm Z}$	$\lvert d_{xy}\rangle$	$\lvert d_{xz}\rangle$	$\lvert d_{yz}\rangle$
$\langle d_{xy}\rvert$	$E_{t_{2g}}$	0	0
$\langle d_{xz}\rvert$	0	$E_{t_{2g}}$	$-i\mu_{\rm B}B$
$\langle d_{yz}\rvert$	0	$i\mu_{\rm B}B$	$E_{t_{2g}}$

This Hamiltonian is trivially diagonal on the basis set

$$\begin{aligned} &|d_{xy}\rangle \\ &|2,+1\rangle = -\frac{1}{\sqrt{2}}\left[|d_{xz}\rangle + i|d_{yz}\rangle\right] \\ &|2,-1\rangle = \frac{1}{\sqrt{2}}\left[|d_{xz}\rangle - i|d_{yz}\rangle\right] \end{aligned} \tag{2.16}$$

with ordered eigenvalues

$$\begin{aligned} E_{d_{xy}} &= E_{t_{2g}} \\ E_{2,+1} &= E_{t_{2g}} + \mu_{\rm B}B \\ E_{2,-1} &= E_{t_{2g}} - \mu_{\rm B}B\,. \end{aligned} \tag{2.17}$$

34. CLEBSCH-GORDAN COEFFICIENTS, SPHERICAL HARMONICS, AND *d* FUNCTIONS

Note: A square-root sign is to be understood over *every* coefficient, *e.g.*, for −8/15 read $-\sqrt{8/15}$.

Notation:

J	J	…
M	M	…

m_1	m_2	
m_1	m_2	Coefficients
.	.	
.	.	
.	.	

1/2 × 1/2

	1	+1	1
+1/2 +1/2	1		

	1	0	0	
+1/2 −1/2	1/2	1/2	1	
−1/2 +1/2	1/2	−1/2	−1	
	−1/2 −1/2	1		

$$Y_1^0 = \sqrt{\frac{3}{4\pi}}\cos\theta$$

$$Y_1^1 = -\sqrt{\frac{3}{8\pi}}\sin\theta\, e^{i\phi}$$

$$Y_2^0 = \sqrt{\frac{5}{4\pi}}\left(\frac{3}{2}\cos^2\theta - \frac{1}{2}\right)$$

$$Y_2^1 = -\sqrt{\frac{15}{8\pi}}\sin\theta\cos\theta\, e^{i\phi}$$

$$Y_2^2 = \frac{1}{4}\sqrt{\frac{15}{2\pi}}\sin^2\theta\, e^{2i\phi}$$

2 × 1/2

	5/2	+5/2	1	
+2 +1/2	1			

	5/2	5/2	3/2		
+2 −1/2	1/5	4/5	5/2	3/2	
+1 +1/2	4/5	−1/5	+1/2	+1/2	
	+1 −1/2	2/5	3/5	5/2	3/2
	0 +1/2	3/5	−2/5	−1/2	−1/2

		5/2	5/2	3/2		
	0 −1/2	3/5	2/5	5/2	3/2	
	−1 +1/2	2/5	−3/5	−3/2	−3/2	
		−1 −1/2	4/5	1/5	5/2	
		−2 +1/2	1/5	−4/5	−5/2	
			−2 −1/2		1	

1 × 1/2

	3/2	+3/2	1
+1 +1/2	1		

	3/2	1/2		
+1 −1/2	1/3	2/3	3/2	1/2
0 +1/2	2/3	−1/3	−1/2	−1/2
	0 −1/2	2/3	1/3	3/2
	−1 +1/2	1/3	−2/3	−3/2
		−1 −1/2		1

3/2 × 1/2

	2	+2	1	
+3/2 +1/2	1			

	2	1			
+3/2 −1/2	1/4	3/4	2	1	
+1/2 +1/2	3/4	−1/4	0	0	
	+1/2 −1/2	1/2	1/2	2	1
	−1/2 +1/2	1/2	−1/2	−1	−1
		−1/2 −1/2	3/4	1/4	2
		−3/2 +1/2	1/4	−3/4	−2
			−3/2 −1/2		1

2 × 1

	3	+3	2	
+2 +1	1			

	3	2			
+2 0	1/3	2/3	3	2	1
+1 +1	2/3	−1/3	+1	+1	+1
	+2 −1	1/15	1/3	3/5	
	+1 0	8/15	1/6	−3/10	
	0 +1	2/5	−1/2	1/10	

		3	2	1		
	+1 −1	1/5	1/2	3/10		
	0 0	3/5	0	−2/5		
	−1 +1	1/5	−1/2	3/10		
		0 −1	2/5	1/2	1/10	
		−1 0	8/15	−1/6	−3/10	
		−2 +1	1/15	−1/3	3/5	

3/2 × 1

	5/2	+5/2	1
+3/2 +1	1		

	5/2	3/2		
+3/2 0	2/5	3/5	5/2	3/2	1/2
+1/2 +1	3/5	−2/5	+1/2	+1/2	+1/2
	+3/2 −1	1/10	2/5	1/2	
	+1/2 0	3/5	1/15	−1/3	
	−1/2 +1	3/10	−8/15	1/6	

		5/2	3/2	1/2		
	+1/2 −1	3/10	8/15	1/6		
	−1/2 0	3/5	−1/15	−1/3		
	−3/2 +1	1/10	−2/5	1/2		
		−1/2 −1	3/5	2/5	5/2	
		−3/2 0	2/5	−3/5	−5/2	
			−3/2 −1		1	

		3	2	1		
	−1 −1	2/5	1/2	1/10		
	−1 0	8/15	−1/6	−3/10		
	−2 +1	1/15	−1/3	3/5		
		−1 −1	2/3	1/3	3	
		−2 0	1/3	−2/3	−3	
			−2 −1		1	

1 × 1

	2	+2	1
+1 +1	1		

	2	1		
+1 0	1/2	1/2	2	1
0 +1	1/2	−1/2	0	0

		2	1		
	+1 −1	1/6	1/2	1/3	
	0 0	2/3	0	−1/3	
	−1 +1	1/6	−1/2	1/3	
		0 −1	1/2	1/2	2
		−1 0	1/2	−1/2	−2
			−1 −1		1

$$Y_\ell^{-m} = (-1)^m Y_\ell^{m*}$$

$$d^\ell_{m,0} = \sqrt{\frac{4\pi}{2\ell+1}}\, Y_\ell^m\, e^{-im\phi}$$

$$\langle j_1 j_2 m_1 m_2 | j_1 j_2 J M\rangle = (-1)^{J-j_1-j_2}\langle j_2 j_1 m_2 m_1 | j_2 j_1 J M\rangle$$

$$d^j_{m',m} = (-1)^{m-m'} d^j_{m,m'} = d^j_{-m,-m'}$$

3/2 × 3/2

	3	+3	1
+3/2 +3/2	1		

	3	2		
+3/2 +1/2	1/2	1/2	3	2	1
+1/2 +3/2	1/2	−1/2	+1	+1	+1
	+3/2 −1/2	1/5	1/2	3/10	
	+1/2 +1/2	3/5	0	−2/5	
	−1/2 +3/2	1/5	−1/2	3/10	

		3	2	1	0	
	+3/2 −3/2	1/20	1/4	9/20	1/4	
	+1/2 −1/2	9/20	1/4	−1/20	−1/4	
	−1/2 +1/2	9/20	−1/4	−1/20	1/4	
	−3/2 +3/2	1/20	−1/4	9/20	−1/4	
		+1/2 −3/2	1/5	1/2	3/10	
		−1/2 −1/2	3/5	0	−2/5	
		−3/2 +1/2	1/5	−1/2	3/10	
			−1/2 −3/2	1/2	1/2	3
			−3/2 −1/2	1/2	−1/2	−3
				−3/2 −3/2		1

$$d^1_{0,0} = \cos\theta \qquad d^{1/2}_{1/2,1/2} = \cos\frac{\theta}{2} \qquad d^1_{1,1} = \frac{1+\cos\theta}{2}$$

$$d^{1/2}_{1/2,-1/2} = -\sin\frac{\theta}{2} \qquad d^1_{1,0} = -\frac{\sin\theta}{\sqrt{2}}$$

$$d^1_{1,-1} = \frac{1-\cos\theta}{2}$$

2 × 3/2

	7/2	+7/2	1
+2 +3/2	1		

	7/2	5/2		
+2 +1/2	3/7	4/7	7/2	5/2	3/2
+1 +3/2	4/7	−3/7	+3/2	+3/2	+3/2
	+2 −1/2	1/7	16/35	2/5	
	+1 +1/2	4/7	1/35	−2/5	
	0 +3/2	2/7	−18/35	1/5	

		7/2	5/2	3/2	1/2	
	+2 −3/2	1/35	6/35	2/5	2/5	
	+1 −1/2	12/35	5/14	0	−3/10	
	0 +1/2	18/35	−3/35	−1/5	1/5	
	−1 +3/2	4/35	−27/70	2/5	−1/10	

		7/2	5/2	3/2	1/2	
	+1 −3/2	4/35	27/70	2/5	1/10	
	0 −1/2	18/35	3/35	−1/5	−1/5	
	−1 +1/2	12/35	−5/14	0	3/10	
	−2 +3/2	1/35	−6/35	2/5	−2/5	

		7/2	5/2	3/2		
	0 −3/2	2/7	18/35	1/5		
	−1 −1/2	4/7	−1/35	−2/5		
	−2 +1/2	1/7	−16/35	2/5		
		−1 −3/2	4/7	3/7	7/2	
		−2 −1/2	3/7	−4/7	−7/2	
			−2 −3/2		1	

2 × 2

	4	+4	1
+2 +2	1		

	4	3		
+2 +1	1/2	1/2	4	3	2
+1 +2	1/2	−1/2	+2	+2	+2
	+2 0	3/14	1/2	2/7	
	+1 +1	4/7	0	−3/7	
	0 +2	3/14	−1/2	2/7	

		4	3	2	1	
	+2 −1	1/14	3/10	3/7	1/5	
	+1 0	3/7	1/5	−1/14	−3/10	
	0 +1	3/7	−1/5	−1/14	3/10	
	−1 +2	1/14	−3/10	3/7	−1/5	

		4	3	2	1	0
	+2 −2	1/70	1/10	2/7	2/5	1/5
	+1 −1	8/35	2/5	1/14	−1/10	−1/5
	0 0	18/35	0	−2/7	0	1/5
	−1 +1	8/35	−2/5	1/14	1/10	−1/5
	−2 +2	1/70	−1/10	2/7	−2/5	1/5

		4	3	2	1	
	+1 −2	1/14	3/10	3/7	1/5	
	0 −1	3/7	1/5	−1/14	−3/10	
	−1 0	3/7	−1/5	−1/14	3/10	
	−2 +1	1/14	−3/10	3/7	−1/5	

		4	3	2		
	0 −2	3/14	1/2	2/7		
	−1 −1	4/7	0	−3/7		
	−2 0	3/14	−1/2	2/7		
		−1 −2	1/2	1/2	4	
		−2 −1	1/2	−1/2	−4	
			−2 −2		1	

$$d^{3/2}_{3/2,3/2} = \frac{1+\cos\theta}{2}\cos\frac{\theta}{2}$$

$$d^{3/2}_{3/2,1/2} = -\sqrt{3}\frac{1+\cos\theta}{2}\sin\frac{\theta}{2} \qquad d^2_{2,2} = \left(\frac{1+\cos\theta}{2}\right)^2$$

$$d^{3/2}_{3/2,-1/2} = \sqrt{3}\frac{1-\cos\theta}{2}\cos\frac{\theta}{2} \qquad d^2_{2,1} = -\frac{1+\cos\theta}{2}\sin\theta$$

$$d^{3/2}_{3/2,-3/2} = -\frac{1-\cos\theta}{2}\sin\frac{\theta}{2} \qquad d^2_{2,0} = \frac{\sqrt{6}}{4}\sin^2\theta \qquad d^2_{1,1} = \frac{1+\cos\theta}{2}(2\cos\theta - 1)$$

$$d^{3/2}_{1/2,1/2} = \frac{3\cos\theta - 1}{2}\cos\frac{\theta}{2} \qquad d^2_{2,-1} = -\frac{1-\cos\theta}{2}\sin\theta \qquad d^2_{1,0} = -\sqrt{\frac{3}{2}}\sin\theta\cos\theta$$

$$d^{3/2}_{1/2,-1/2} = -\frac{3\cos\theta + 1}{2}\sin\frac{\theta}{2} \qquad d^2_{2,-2} = \left(\frac{1-\cos\theta}{2}\right)^2 \qquad d^2_{1,-1} = \frac{1-\cos\theta}{2}(2\cos\theta + 1) \qquad d^2_{0,0} = \left(\frac{3}{2}\cos^2\theta - \frac{1}{2}\right)$$

Figure 34.1: The sign convention is that of Wigner (*Group Theory*, Academic Press, New York, 1959), also used by Condon and Shortley (*The Theory of Atomic Spectra*, Cambridge Univ. Press, New York, 1953), Rose (*Elementary Theory of Angular Momentum*, Wiley, New York, 1957), and Cohen (*Tables of the Clebsch-Gordan Coefficients*, North American Rockwell Science Center, Thousand Oaks, Calif., 1974). The coefficients here have been calculated using computer programs written independently by Cohen and at LBNL.